11th International Symposium on Turbulence and Shear Flow Phenomena (TSFP11)
Southampton, UK, July 30 to August 2, 2019

ATTACHED AND DETACHED STRUCTURES IN A TURBULENT BOUNDARY LAYER SUBJECTED TO ADVERSE PRESSURE GRADIENT

Min Yoon

Dept. of Mechanical Engineering
KAIST
Daejeon 34141, Korea
minyoon@kaist.ac.kr

Jinyul Hwang

Dept. of Mechanical Engineering
KAIST
Daejeon 34141, Korea
j.yhwang@kaist.ac.kr

Jongmin Yang

Dept. of Mechanical Engineering
KAIST
Daejeon 34141, Korea
asyligo@kaist.ac.kr

Hyung Jin Sung

Dept. of Mechanical Engineering
KAIST
Daejeon 34141, Korea
hjsung@kaist.ac.kr

ABSTRACT

Three-dimensional clusters of the streamwise velocity fluctuations (u) are explored in a view of the attached-eddy model, which provides a basis for understanding asymptotic behaviors at high-Reynolds-number wall turbulence in terms of coherent structures. We extract u clusters using the direct numerical simulation data of boundary layers subjected to adverse and zero pressure gradients. The identified structures are decomposed into attached self-similar, attached non-self-similar, detached self-similar and detached non-self-similar motions with respect to the minimum distance from the wall ($y_{\min}$) and height (l_y). The attached structures ($y_{\min} \approx 0$) are main enegy-containing motions in which they carry approximately a half of the streamwise Reynolds stress and the Reynolds shear stress in the logarithmic and outer regions. The sizes of attached self-similar structures scale with l_y and their population density exhibits an inverse-scale distribution over $0.3\delta < l_y < 0.6\delta$ (δ is the 99% boundary layer thickness). They also contirbute to the logarithmic variation of the streamwise Reynolds stress; i.e., these structures are universal wall motions in the logarithmic region. The tall attached structures with $l_y = O(\delta)$ are non-self-similar and responsible for the outer enhanced large scales under the adverse pressure gradient. They extend over 6δ in the stremwise direction and peneterate deeply into the near-wall region, reminiscent of superstructures or very-large-scale motions. Detached self-similar structures ($y_{\min} > 0$ and $l_y > 100\nu/u_\tau$) are geometrically isotropic and mainly populated in the outer region while the sizes of detached non-self-similar structures ($y_{\min} > 0$ and $l_y^+ < 100$) are scaled by Kolmogorov length scale. The present study can provide a new perspective on the analysis of turbulence structures in the view of the attached-eddy model.

INTRODUCTION

Townsend (1976) deduced that energy-containing motions in the logarithmic region in wall-bounded turbulent flows are organized by a linear superposition of self-similar eddies that are attached to the wall. The size of each eddy is proportional to the distance from the wall (y). Townsend's attached-eddy hypothesis predicts turbulence statistics in the logarithmic region in the sense of the structures: i.e., the logarithmic variation in the wall-parallel components of the Reynolds stresses. A typical feature of turbulent boundary layers (TBLs) subjected to adverse pressure gradients (APGs) is the enhancement of large-scale energy above the logarithmic region. A strong outer peak is observed in the streamwise Reynolds stress, which results from long-wavelength motions in energy spectra (Harun *et al*. 2013; Lee 2017; Yoon *et al*. 2018). The large-scale motions (LSMs) with $O(\delta)$ in the logarithmic region, where δ is the 99% boundary layer thickness, influence small-scale motions through the amplitude modulation (Hutchins & Marusic 2007*b*; Hwang *et al*. 2016*a*,*b*) and are extended to the near-wall region as footprints (Hoyas & Jiménez 2006; Hutchins & Marusic 2007*a*). Recently, Hwang & Sung (2018) reported that the wall-attached structures of streamwise velocity fluctuations (u) are self-similar and contribute to the presence of the logarithmic layer in a zero pressure gradient (ZPG) TBL. Therefore, a research on Townsend's attached-eddy hypothesis in APG TBLs is demanded through the wall-attached u structures to predict turbulence statistics influenced by strengthened LSMs. Although extensive studies of turbulence statistics in APG TBLs have been performed, much attention has not been paid to wall-attached structures despite its importance.

The concept of attached eddies originates in the idea of Townsend (1976) who proposed a double-cone vortex model for the energy-containing motions in the logarithmic region whose sizes are proportional to y; *attached* to the wall. The wall-attached structures are self-similar and are superimposed by eddies of different sizes with a constant characteristics velocity. In the logarithmic region, the Reynolds normal stresses can be expressed in the sense of Townsend's attached-eddy hypothesis: $\langle uu\rangle/u_\tau^2 = B_1 - A_1 \ln(y/\delta)$, $\langle ww\rangle/u_\tau^2 = B_2 - A_2 \ln(y/\delta)$ and $\langle vv\rangle/u_\tau^2 = B_3$, where $\langle uu\rangle$, $\langle vv\rangle$ and $\langle ww\rangle$ are the streamwise, wall-normal and spanwise components of the Reynolds stresses, respectively; u_τ is the friction velocity, and A_1, A_2, B_1, B_2 and B_3 are constants. Perry & Chong (1982) extended Townsend's attached-eddy hypothesis to their model, where a hierarchy of geometrically similar eddies is randomly distributed with a population density that is inversely proportional to their height, leading to the logarithmic variation of $\langle uu\rangle^+$ and $\langle ww\rangle^+$, where the superscript + denotes non-dimensionalization by the wall variables. Accordingly, attached-eddy models explain the asymptotic behaviors of the turbulence statistics at high-Reynolds-number turbulent flows in terms of coherent structures.

After the 2000s, several studies of high-Reynolds-number wall-bounded turbulent flows ($Re_\tau > O(10^4)$) have been performed owing to the development of experimental equipment and computational power. Here, Re_τ is the friction Reynolds number ($= u_\tau\delta/\nu$, where ν is the kinematic viscosity). The role of wall-attached structures becomes significant as the increase in the Reynolds number. For instance, the logarithmic behavior in $\langle uu\rangle^+$ is observed in ZPG TBLs at $Re_\tau = O(10^4)$ (Hutchins *et al.* 2009; Vallikivi *et al.* 2015; Baidya *et al.* 2017; Samie *et al.* 2018), atmospheric surface layer at $Re_\tau = O(10^6)$ (Hutchins *et al.* 2012), turbulent pipe flow at $Re_\tau = O(10^{4-5})$ (Hultmark *et al.* 2012; Örlü *et al.* 2017) and turbulent channel flow at Re_τ = 5200 (Lee & Moser 2015).

Several models have been made by extending the model of Perry & Chong (1982). Perry *et al.* (1986) modified the inverse power-law in the population density of attached eddies by increasing the weighting for those with δ-height to accurately predict the velocity defect law and the energy distribution in low-wavenumber region. Despite the modification for large scales (Perry *et al.* 1986), a significant difference is observed between the experimental data and the model prediction in APG TBLs, especially in the Reynolds stresses in the outer region. Perry & Marusic (1995) recognized that another eddy with a different shape is needed for describing the Reynolds stresses in APG TBLs; the wall−wake attached-eddy model is proposed, comprised of wall-attached eddies (type A), larger detached eddies with $O(\delta)$ (type B) and smaller detached eddies including Kolmogorov scales (type C). Type-B eddies whose sizes are scaled with their height are mainly populated in the outer region, and they are modeled by trial and error. Studies of large scales in the outer region have proposed a new point of view on the larger detached structures (Smits *et al.* 2011). Details of the model are summarized in Marusic & Monty (2019). Hwang & Sung (2018) observed the inverse-power-law distribution of the wall-attached *u* structures and the outer peak in the population density, representing to the additional weighting for large scales as conjectured by Perry *et al.* (1986). Hence, it is necessary to decompose coherent *u* structures in the sense of the attached-eddy models to understand the multiscale nature of wall turbulence.

Recently, increasing attention has been paid to coherent structures in APG TBLs. The hairpin packets are more inclined away from the wall (Lee & Sung 2009) and the inclination angle increases as the increase in the strength of APG (Lee 2017). The long *u* streaks with $O(\delta)$ shrank, and the lengths of negative-*u* structures are widened in the outer region (Lee & Sung 2009). It would be difficult in previous studies to discriminate whether coherent structures are attached to the wall or detached from that. To overcome this limitation, vortical clusters (del Álamo *et al.* 2006) and ejection and sweeps (Lozano-Durán *et al.* 2012) are extracted in DNS of channel flows. The identified structures are divided into wall-attached or wall-detached on the basis of the minimum distance from the wall. These wall-attached structures are self-similar and dominantly contribute turbulence statistics in the logarithmic region. Subsequently, Maciel *et al.* (2017*a*,*b*) analyzed individual cluster in APG TBLs by identifying ejection and sweeps. The self-similar wall-attached ejection and sweeps in APG TBLs carry 30−45% of $\langle -uv\rangle$ in the region of y/δ = 0.2 ~ 0.8, which is larger than that (25−40%) of ZPG TBL. Since self-similar structures in APG TBLs play a major role in the energy-containing motions, especially in the outer region, it is essential to analyze coherent *u* structures in APG TBLs by decomposing them in the sense of attached-eddy models.

The objective of the present study is to explore three-dimensional (3D) clusters of streamwise velocity fluctuations (*u*) by decomposing them in the view of Townsend's attached-eddy hypothesis. Toward this end, direct numerical simulation (DNS) data of an APG and ZPG TBLs at $Re_\tau \approx 800$ are used. The identified structures are classified into attached self-similar (type A, wall-scaling), attached non-self-similar (type B, outer-scaling) and self-similar/non-self-similar detached structures (viscous-scaling) according to the height (l_y) of the objects.

NUMERICAL DETAILS

In the present study, DNS dataset of an APG TBL (Yoon *et al*. 2018) is used. The continuity equation and the Navier−Stokes equations for incompressible flows are discretized using the fractional step method of Kim *et al.* (2002) to perform DNS of an APG TBL. The computational domain sizes are $1834\delta_0 \times 100\delta_0 \times 130\delta_0$ in the streamwise (*x*), wall-normal (*y*) and spanwise (*z*) directions, respectively. Here, δ_0 is the inlet boundary layer thickness. The number of the grid is 10497 (*x*) × 541 (*y*) × 1025 (*z*), and *u*, *v* and *w* indicate the streamwise, wall-normal and spanwise velocity fluctuations, respectively. For comparison, DNS dataset of a ZPG TBL (Hwang & Sung 2017) is included. Details of the numerical procedure and the boundary conditions can be found in Yoon *et al.* (2018). The domain of interest (DoI) is chosen as 10δ (*x*) × 1.2δ (*y*) × 3δ (*z*). Figure 1 shows the skin friction coefficient (C_f) and 3D iso-surface of *u*, where color contour indicates DoI. Details of the information of DoI are listed in table 1.

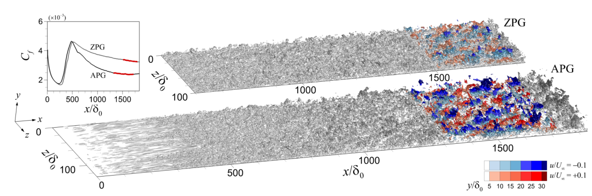

Figure 1. Skin friction coefficient (C_f) and 3D iso-surface. Red line in C_f and color contours in iso-surface indicate DoI.

Table 1. Information of DoI. The number in brackets indicates the center value at DoI (circle symbols in figure 1*b*,*c*). δ_x, δ_y and δ_z are the streamwise, wall-normal and spanwise sizes of DoI, respectively.

	APG	ZPG
x/δ_0	1318.6 ~ 1719.7	1509.5 ~ 1796.8
Re_τ	680 ~ 873 (775)	769 ~ 884 (825)
Re_θ	4050 ~ 5700 (4860)	2260 ~ 2654 (2457)
δ/δ_0	32.75 ~ 46.05 (39.3)	23.32 ~ 27.42 (25.3)
δ_x/δ	10.2	11.4
δ_y/δ	1.2	1.1
δ_z/δ	3.31	3.95

The coherent structures of *u* are defined as the groups of connected points of $u(\mathbf{x}) > \alpha u_{rms}(y)$ and $u(\mathbf{x}) < -\alpha u_{rms}(y)$, where α is the threshold and u_{rms} is the root mean square of *u*. To detect each *u* cluster, we use the connectivity of neighboring six-orthogonal grids at a given node in Cartesian coordinates (del Álamo *et al*. 2006; Lozano-Durán *et al*. 2012; Hwang & Sung 2018). By using this method, we can obtain the spatial information of individual *u* cluster. In order to choose α, a percolation diagram for the identified *u* clusters is shown in figure 2(*a*). The total number (*N*) and total volume (*V*) at certain

α are normalized by the maximum N (N_{max}) and V (V_{max}), respectively. The normalized volume (V/V_{max}) increases as the decrease in α and in particular it significantly changes over 1.2 < α < 1.7, indicating the presence of the percolation crisis. Within this region, the number ratio (N/N_{max}) shows a peak at α = 1.5. The variations of V/V_{max} and N/N_{max} in the APG and ZPG TBLs collapse well, representing that the percolation behavior of u clusters is independent of the pressure gradient. In the present study, we select α = 1.5.

Figure 2(b) represents the number of u clusters per unit wall-parallel area ($A_{xz} = \delta_x\delta_z$) as a function of y_{min} and y_{max}, which are the minimum and maximum distances from the wall: $n^* = n(y_{min}, y_{max})/(mA_{xz})$, where n is the number of identified u clusters and m is the number of instantaneous flow fields used to detect u clusters. Here, color and line contours of n^* denote the APG and ZPG, respectively. The u clusters with the volume larger than 30^3 wall units are only analyzed (del Álamo *et al.* 2006). All u structures are divided into two groups; one is observed at $y^+_{min} \approx 0$ and the other is at $y^+_{min} \gg 0$, indicating wall-attached and wall-detached structures, respectively. With the present criteria (i.e., $y^+_{min} \approx 0$), we can analyze the wall-normal variations of the turbulence statistics carried by these structures according to their height (l_y) without any interpolation since $l_y = y_{max}$.

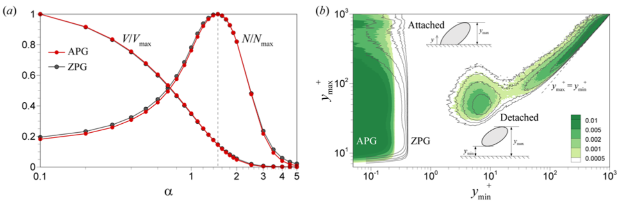

Figure 2. (a) Percolation diagram of detected u clusters. The total volume (V) and total number (N) of clusters vary with respect to α. (b) The number of u clusters per unit wall-parallel area (n^*) with respect to y_{min} and y_{max}.

We examine the contribution of the attached and detached u structures to $\langle uu\rangle$. Figure 3(a) exhibits the profiles of $\langle uu\rangle^+$, where the magnitude of $\langle uu\rangle^+$ in the outer region is enhanced with a presence of a secondary peak near y^+ = 240 in the APG TBL (red line). The streamwise Reynolds stresses carried by the attached and detached u structures are presented in figure 3(b), and they are defined as

$$\langle uu\rangle_{\text{attached}}(y) = \frac{1}{mV_{\text{DoI}}}\int_{\Omega_{\text{attached}}} u(\mathbf{x})u(\mathbf{x})\mathrm{d}\mathbf{x} \qquad (1)$$

$$\langle uu\rangle_{\text{detached}}(y) = \frac{1}{mV_{\text{DoI}}}\int_{\Omega_{\text{detached}}} u(\mathbf{x})u(\mathbf{x})\mathrm{d}\mathbf{x} \qquad (2)$$

where $\Omega_{attached}$ and $\Omega_{detached}$ are the domain of all constituent points of attached and detached structures, respectively, and V_{DoI} (= $\delta_x\delta_y\delta_z$) is the volume of DoI. The attached u structures account for over half of $\langle uu\rangle^+$, whereas the detached u structures contribute to less than 13% of $\langle uu\rangle^+$. In addition, the shape of $\langle uu\rangle^+_{\text{attached}}$ is similar to that of $\langle uu\rangle^+$. The wall-normal location of the inner peak of $\langle uu\rangle^+_{\text{attached}}$ appears at $y^+ \approx 15$ and the outer peak of $\langle uu\rangle^+_{\text{attached}}$ is observed at y^+ = 210. In contrast to $\langle uu\rangle^+_{\text{attached}}$, the profiles of $\langle uu\rangle^+_{\text{detached}}$ in the APG and ZPG TBLs collapse well up to y^+ = 100. At y^+ > 100, the magnitude of $\langle uu\rangle^+_{\text{detached}}$ in the APG is larger than that in the ZPG and there is an outer peak at y/δ = 0.5, respectively. This result indicates that the detached structures within y^+ < 100 do not affected by the pressure gradient. In the present study, the identified wall-attached structures carry approximately half of $\langle uu\rangle^+$, representing that they are the main energy-containing motions.

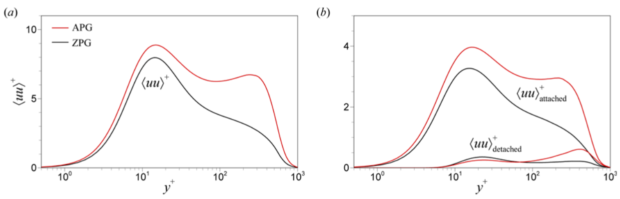

Figure 3. (a) $\langle uu\rangle^+$ and (b) $\langle uu\rangle^+_{\text{attached}}$ and $\langle uu\rangle^+_{\text{detached}}$.

WALL-ATTACHED STRUCTURES

In this section, we explore the identified attached structures by focusing on the eddy models proposed by Perry & Marusic (1995). They suggested three types of eddies. First, the type-A eddies are self-similar and the main energy-containing motions in the log region. In this sense, these eddies are universal structures in wall turbulence. The type-B eddies are characterized by the boundary layer thickness and responsible for the turbulence statistics in the outer region and the low-wavenumber energy. Perry & Marusic (1995) conjectured the type-B eddies to model the outer peak of the streamwise Reynolds stress in APG because the predicted intensity only considering type-A eddies showed large discrepancies in the outer region. The type-C eddies are associated with the small-scale motions. Although Perry & Marusic (1995) modeled that the type-B eddies are physically detached from the wall, recent studies showed that very-large-scale motions or superstructures are related to type-B eddies since these large-scale structures are characterized by the outer length scale (Hutchins & Marusic 2007b). However, the LSMs penetrate into the near-wall region and impose their footprints (Hutchins & Marusic 2007a), indicating they can physically adhere to the wall. In the present work, we simply decompose the identified turbulence motions based on their height and presents the statistical properties of each motion satisfying the characteristics of type A, B or C motions described in the works of Perry and coworkers.

We examine the population density of the attached u structures (n^*_{attached}) with respect to l_y. Here, n^*_{attached} is defined as the number of attached u structures per unit wall-parallel area with respect to l_y: $n^*_{\text{attached}}(l_y) = n_{\text{attached}}(l_y)/(mA_{xz})$, where $n_{attached}$ is a function of l_y and m is the number of fields. Figure 4(a) shows the distributions of n^*_{attached}. In the APG (red), we can observe the region where n^*_{attached} is inversely proportional to l_y, reminiscent of a hierarchical length-scale distribution of the attached-eddy hypothesis. This region spans over l_y/δ = 0.4 ~ 0.58 (l_y^+ = 310 ~ 450) as shown in the inset of figure 5(a); the best fit of the inverse power-law is $n^*_{\text{attached}} = 0.0026(l_y/\delta)^{-1}$. After the upper limit of the inverse power-law region ($l_y/\delta \approx 0.6$), n^*_{attached} increases and exhibits the peak at l_y/δ = 0.92 (l_y^+ = 710). This behavior indicates the relative dominance of tall attached structures with δ-length height (Perry *et al.* 1986). In addition, the magnitude of the peak in the APG is 1.3 times larger than that in the ZPG, representing that the APG enhance large-scale structures in the outer region (Harun *et al*. 2013; Yoon *et al*. 2018). In addition, the average volume of the attached u structures with $l_y = O(\delta)$ is increased by 16% at that of the ZPG. This behavior could lead to a relatively lower population over $0.3 < l_y/\delta < 0.6$ in the APG. The enhanced population and volume of the tall attached structures have an essential role in the presence of the outer peaks observed in the Reynolds stresses of the APG.

As discussed above, n^*_{attached} clearly follows the population density of attached eddies conjectured by Perry & Chong (1982) and Perry *et al*. (1986). Thus, we decompose the wall-attached structures into two types based on the height of attached u structures: i.e., type A ($100\nu/u_\tau \le l_y \le 0.6\delta$) and type B ($l_y > 0.6\delta$).

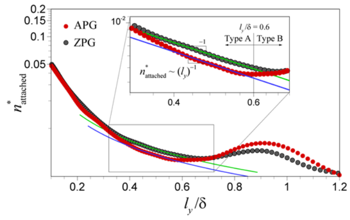

Figure 4. n^*_{attached} with respect to l_y^+. Solid lines indicate $n^*_{\text{attached}} \sim (l_y)^{-1}$. The inset represents an enlarged view in the region $l_y/\delta = 0.32 \sim 0.72$ with a logarithmic abscissa. The inset shows the inverse power-law regions.

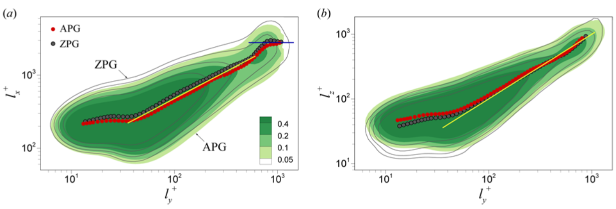

Figure 5. Joint PDFs of (*a*) l_x and l_y and of (*b*) l_z and l_y. Color and line contours indicate APG and ZPG, respectively. Circle symbols are the mean lengths. A yellow solid line in (*a*) is $l_x \sim l_y^{0.74}$ in the region from $l_y^+ = 100$ to $l_y/\delta = 0.6$, and a blue solid line indicates $l_x \approx 3.5\delta$. A yellow solid lines in (*b*) represents $l_z^+ = l_y^+$ at $l_y^+ > 100$.

We explore the length (l_x) and width (l_z) of the wall-attached u structures to examine whether the sizes of the type-A and type-B structures are characterized by l_y and δ, respectively. The length scales of individual structure is defined as the circumscribing box dimensions of an object; i.e., l_x, l_y and l_z are the streamwise, wall-normal and spanwise lengths, respectively. Figure 5(*a*,*b*) represents joint PDFs of l_x and l_z of the wall-attached u structures with respect to l_y. Here, the contour and line contours indicate the distributions of the APG and ZPG, respectively. The mean l_x and l_z at a given l_y are denoted by the inserted cycles; APG (red) and ZPG (black). As shown in figure 5(*a*), the l_x of the type-A structures ($100\nu/u_\tau < l_y < 0.6\delta$) scales with l_y and in particular follows the power law $l_x \sim l_y^{0.74}$ (yellow solid line), in both TBLs. Above $l_y > 0.6\delta$, the l_x rapidly increases and then the mean l_x exhibits a constant value $l_x \approx 3.5\delta$ at $l_y > \delta$ (blue horizontal line), indicating that very tall structures (i.e., type B) are non-self-similar and scale with the outer length scale δ. In addition, the contours show the protrusions near $l_y \approx \delta$, which represent the existence of long attached structures with $l_y > 6\delta$ (i.e., superstructures or very-large-scale motions). In figure 5(*b*), we can observe the linear relationship between l_z and l_y (yellow solid line) from $l_y^+ = 100$ to $l_y = \delta$. In other words, the spanwise length of the attached u structures ($l_y^+ > 100$) is proportional to the distance from the wall, which is consistent with the results of Hwang (2015) that large-scale and very-large-scale motions are self-similar with respect to the spanwise wavelength. In particular, the width distributions of the APG and ZPG collapse well, reflecting that the spanwise length scales of attached u structures will not be significantly modulated by the APG. In sum, the type-A structures are geometrically self-similar with respect to l_y whereas the streamwise length of the type-B motions scales with the outer length scale.

The streamwise Reynolds stresses and the Reynolds shear stresses carried by type A and type B are defined as

$$\langle uu \rangle_{\text{A}}(y) = \frac{1}{mV_{\text{DoI}}} \sum_{l_y^+=100}^{l_y/\delta=0.6} \int_{\Omega_{\text{attached}}(l_y)} u(\mathbf{x})u(\mathbf{x})\mathrm{d}\mathbf{x}, \qquad (3)$$

$$\langle uu \rangle_{\text{B}}(y) = \frac{1}{mV_{\text{DoI}}} \sum_{l_y/\delta=0.6}^{l_y=\delta_y} \int_{\Omega_{\text{attached}}(l_y)} u(\mathbf{x})u(\mathbf{x})\mathrm{d}\mathbf{x}. \qquad (4)$$

Figure 6(*a*) shows the wall-normal profiles of $\langle uu \rangle^+_{\text{A}}$ in the APG (red) and ZPG (black). Interestingly, both profiles are self-similar along the wall-normal direction and in particular there is a logarithmic variation over $100 < y^+ < 250$. This behavior supports that the attached u structures ($100\nu/u_\tau < l_y < 0.6\delta$) correspond to the type-A eddies (Perry & Marusic 1995). In other words, these structures are universal motions and directly contribute to the presence of the log region. Contrary to $\langle uu \rangle^+_{\text{A}}$, $\langle uu \rangle^+_{\text{B}}$ of the APG is entirely different from that of ZPG with a distinct outer peak at $y^+ = 230$ (figure 6*b*). The enhanced streamwise Reynolds stress carried by the attached u structures in the APG ($\langle uu \rangle^+_{\text{attached}}$ shown in figure 3*b*) is due to the contribution of the type-B structures ($l_y > 0.6\delta$). Moreover, the magnitude of the outer peak ($y^+ \approx 240$) is greater than that of the inner peak at $y^+ \approx 15$, reflecting that the attached u structures with $l_y > 0.6\delta$ are responsible for the wake region. In addition, there is no logarithmic variation in $\langle uu \rangle^+_{\text{B}}$, indicating that the tall attached u structures are associated with very-large-scale motions or superstructures (Jiménez & Hoyas 2008).

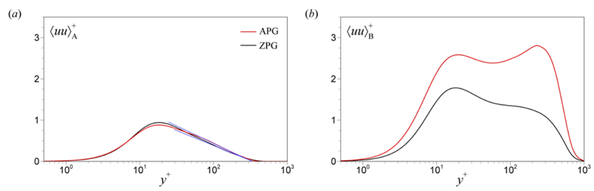

Figure 6. (*a*) $\langle uu \rangle^+_{\text{A}}$ and (*b*) $\langle uu \rangle^+_{\text{B}}$. (*c*) $\langle -uv \rangle^+_{\text{A}}$ and $\langle -uv \rangle^+_{\text{B}}$. The solid line represents the logarithmic variation in $\langle uu \rangle^+_i$: $\langle uu \rangle^+_{\text{A}} = -0.37\ln(y^+) + 2.12$ in $y^+ = 100 \sim 250$ for APG and $\langle uu \rangle^+_{\text{A}} = -0.32\ln(y^+) + 1.84$ in $y^+ = 100 \sim 250$ for ZPG.

WALL-DETACHED STRUCTURES

In this section, we examine the detached structures of u, which account for 50.0% of the total volume of u clusters in the APG and ZPG TBLs. In addition, the contributions of the detached u structures to the Reynolds stresses show a good agreement at $y^+ < 100$ between the APG and ZPG, whereas there is a large discrepancy above $y^+ = 100$ in figure 3(*b*). To further explore this difference, we investigate the detached structures with respect to their sizes and the wall-normal location (y_c). Here, $y_c = (y_{min} + y_{max})/2$ is the center of the detached structures from the wall.

First, the number wall-detached structures per unit wall-parallel area (n^*_{detached}) is defined as $n^*_{\text{detached}} = n_{\text{detached}}(l_y, y_c)/(mA_{xz})$, where n_{detached} is the number of detached structures as a function of y_c and l_y. As shown in figure 4(*b*), the magnitudes of $\langle uu\rangle^+_{\text{detached}}$ and $\langle -uv\rangle^+_{\text{detached}}$ are larger in the region of $y^+ > 100$ than those of ZPG. Hence, we focus on the detached structures with $y_c^+ > 100$. Figure 8 shows n^*_{detached} with respect to l_y^+ and y_c^+ for APG (color contour) and ZPG (line contour). As y_c^+ increases, n^*_{detached} increases and the range of their heights becomes broader from $l_y^+ = 10$ to $l_y/\delta = 0.7$. In addition, a peak is observed at $y_c^+ = 550$ and $l_y^+ = 60$, indicating the detached *u* structures are dominant in the outer region.

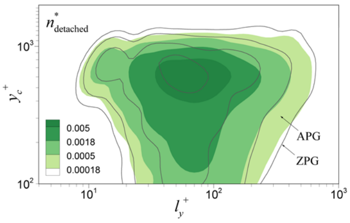

Figure 7. Contour maps of n^*_{detached} for APG (color) and ZPG (line) as a function of l_y^+ and y_c^+.

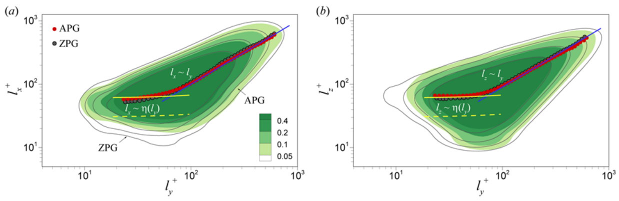

Figure 8. Joint PDFs of (*a*) l_x and l_y and of (*b*) l_z and l_y of type-C structures. Color and line contours indicate APG and ZPG, respectively. Circle symbols are the mean lengths. Green solid lines indicate $l_x = l_y$ in (*a*) and $l_z = 0.9l_y$ in (*b*). Yellow solid and dashed lines in (*a*,*b*) represent $l_y = 40\eta$ and 20η of APG, respectively.

Figure 8 shows joint PDFs of l_x and l_y and of l_z and l_y of the detached structures. As seen, the contours of the APG and ZPG collapse well, indicating that the sizes of the detached structures are universal. There are two regions, representing that the detached *u* structures are classified into self-similar and non-self-similar groups. Above $l_y^+ = 100$, the mean l_x and l_z (inserted circles) are linearly proportional to l_y, and in particular the aspect ratio of their sizes follow $l_x \approx l_y \approx l_z$, indicating that the tall detached structures ($l_y^+ > 100$) are geometrically isotropic and self-similar with respect to their sizes. This result is similar to the sizes of detached sweep and ejections which follow the ratio $l_x \approx 1.2l_y \approx 1.2l_z$ in APG and ZPG TBLs (Maciel *et al.* 2017*b*). On the other hand, the detached motions with $l_y^+ < 100$ follow the yellow solid lines $l_x = 40\eta(l_y)$ and $l_z = 40\eta(l_y)$ (figure 8), where η is the Kolmogorov length scale. In other words, these motions are not self-similar according to l_y. In addition, the yellow dashed line ($l_x \sim l_z \sim 20\eta$) lies on the contour of over 0.05. This observation is consistent with the length scales ($\sim 20{-}40\eta$) of detached vortical clusters (del Álamo *et al.* 2006) and detached sweep and ejections (Lozano-Durán *et al.* 2012). Hence, the short detached *u* structures ($l_y^+ < 100$) are associated with the Kolmogorov-scale motions and they are equilateral at a given l_y ($l_x = l_z = 40\eta$). The outer peak (at $y_c^+ = 550$ and $l_y^+ = 60$) observed in the population density (figure 7) is due to this type of motions.

To investigate the contributions of short and tall detached *u* structures to $\langle uu\rangle_{\text{detached}}$, we compute $\langle uu\rangle$ carried by the short ($l_y^+ < 100$) and tall ($y^+ > 100$) detached *u* structures, which can be obtained from a similar way with (3) and (4). Figure 9 shows $\langle uu\rangle^+_{\text{short}}$, $\langle uu\rangle^+_{\text{tall}}$ and $\langle uu\rangle^+_{\text{detached}}$ as a function of y/δ. The detached *u* structures with $y_c^+ > 100$ are responsible for $\langle uu\rangle^+_{\text{detached}}$ in the region of $y^+ > 100$ ($y/\delta > 0.13$). As expected above, the tall detached *u* contributes 90% of $\langle uu\rangle^+_{\text{detached}}$ in the region of $y/\delta > 0.2$, while the short objects account for 10% of $\langle uu\rangle^+_{\text{detached}}$. Tall detached structures who are scaled by the viscous length are isotropic and geometrically self-similar. The peak of $\langle uu\rangle^+_{\text{tall}}$ is observed at $y/\delta = 0.53$, and its magnitude is 26% of $\langle uu\rangle^+_{\text{B}}$ at that location. Perry *et al.* (1986) supposed that detached eddies originate from the debris of dead attached eddies, which are advected away from the wall and deformed by attached large scales. In other words, they could be remainders once attached to the wall earlier in their lifetime (Marusic & Monty 2019). Hence, the origin of the tall detached *u* could be fragments of the large-scale attached structures (or type-B structures) in the outer region. To verify this, their temporal variation is necessary, but that is beyond the scope of the present work. On the other hand, the contribution of the short detached structures to $\langle uu\rangle^+$ is too small compared to that of $\langle uu\rangle^+_{\text{tall}}$. However, since the small-scale motions have an important role in dissipation process, these motions should be considered when we explore the dynamics of *u* clusters to examine multiscale energy cascade in wall turbulence.

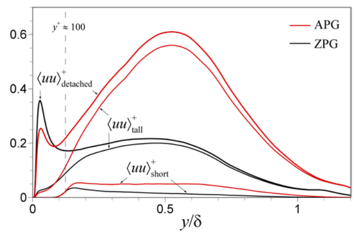

Figure 9. $\langle uu\rangle^+_{\text{short}}$, $\langle uu\rangle^+_{\text{tall}}$ and $\langle uu\rangle^+_{\text{detached}}$ for APG and ZPG.

CONCLUSIONS

3D coherent *u* clusters have been explored in a view of the attached-eddy model. We have extracted *u* clusters by using the connectivity of six-orthogonal neighbors in Cartesian coordinates without any filter and assumption from DNS dataset of APG ($\beta = 1.43$) and ZPG ($\beta = 0$) TBLs at $Re_\tau \approx 800$. The identified structures are decomposed into attached self-similar, attached non-self-similar, detached self-similar and detached non-self-similar structures with respect to y_{min} and l_y.

The wall-attached self-similar structure ($l_y^+ > 100$ and $l_y/\delta < 0.6$) are universal wall motions in the logarithmic region, and their statistical features are equivalent to those of type-A motions in the attached-eddy models of Perry and coworkers. The attached non-self-similar structures ($l_y/\delta > 0.6$) are responsible for the enhanced outer large scales under APG and incorporate the characteristics of tall type-A ($l_y = O(\delta)$) and type-B motions described in the works of Perry and coworkers. On the other hand, the detached self-similar structures ($y_c^+ > 100$ and $l_y^+ > 100$) are geometrically isotropic ($l_x \approx l_y \approx l_z$) and mainly populated in the outer region, while the sizes of the detached non-self-similar structures ($y_c^+ > 100$ and $l_y^+ < 100$) are scaled by the Kolmogorov length scale ($l_x = l_z = 40\eta$). The former structures carry approximately a quarter of $\langle uu\rangle_B^+$ in the outer region, implying that they are the remnants of the attached non-self-similar structures. The present study first classify 3D coherent u clusters into attached/detached and self-similar/non-self-similar, which are in a good agreement with type-A, B and C motions in the attached-eddy model. We examine the statistical properties of each motion and the contirbution of that to $\langle uu\rangle^+$, which can provide a new insight into the understanding of coherent structures and the development of the attached-eddy model.

ACKNOWLEDGMENTS

This study was supported by a grant from the National Research Foundation of Korea (No. 2019M3C1B7025091), and partially supported by the Supercomputing Center (KISTI).

REFERENCES

Baidya, R., Philip, J., Hutchins, N., Monty, J. P., and Marusic, I., 2017, "Distance-from-the-wall scaling of turbulent motions in wall-bounded flows", *Physics of Fluids*, Vol. 29(2), 020712.

del Álamo, J. C., Jiménez, J., Zandonade, P., and Moser, R. D., 2006, "Self-similar vortex clusters in the turbulent logarithmic region", *Journal of Fluid Mechanics*, Vol. 561, pp. 329–358.

Harun, Z., Monty, J. P., Mathis, R., and Marusic, I., 2013, "Pressure gradient effects on the large-scale structure of turbulent boundary layers", *Journal of Fluid Mechanics*, Vol. 715, pp. 477–498.

Hoyas, S., and Jiménez, J., 2006, "Scaling of the velocity fluctuations in turbulent channels up to $Re_\tau = 2003$", *Physics of Fluids*, Vol. 18(1), 011702.

Hultmark, M., Vallikivi, M., Bailey, S. C. C., and Smits, A. J., 2012, "Turbulent pipe flow at extreme Reynolds numbers", *Physical review letters*, Vol. 108(9), 094501.

Hutchins, N., Chauhan, K., Marusic, I., Monty, J., and Klewicki, J., 2012, "Towards reconciling the large-scale structure of turbulent boundary layers in the atmosphere and laboratory", *Boundary-layer meteorology*, Vol. 145(2), 273–306.

Hutchins, N., and Marusic, I., 2007*a*, "Evidence of very long meandering features in the logarithmic region of turbulent boundary layers", *Journal of Fluid Mechanics*, Vol. 579, pp. 1-28.

Hutchins, N., and Marusic, I., 2007*b*, "Large-scale influences in near-wall turbulence", *Philosophical Transactions of the Royal Society of London A: Mathematical, Physical and Engineering Sciences*, Vol. 365(1852), pp. 647–664.

Hutchins, N., Nickels, T. B., Marusic, I., and Chong, M. S., 2009, "Hot-wire spatial resolution issues in wall-bounded turbulence", *Journal of Fluid Mechanics*, Vol. 635, pp. 103–136.

Hwang, J., Lee, J., and Sung, H. J., 2016*a*, "Influence of large-scale accelerating motions on turbulent pipe and channel flows", *Journal of Fluid Mechanics*, Vol. 804, pp. 420–441.

Hwang, J., Lee, J., Sung, H. J., and Zaki, T. A., 2016*b*, "Inner-outer interactions of large-scale structures in turbulent channel flow", *Journal of Fluid Mechanics*, Vol. 790, pp. 128–157.

Hwang, J., and Sung, H. J., 2017, "Influence of large-scale motions on the frictional drag in a turbulent boundary layer", *Journal of Fluid Mechanics*, Vol. 829, pp. 751–779.

Hwang, J., and Sung, H. J., 2018, "Wall-attached structures of velocity fluctuations in a turbulent boundary layer", *Journal of Fluid Mechanics*, Vol. 856, pp. 958–983.

Hwang, J., and Sung, H. J., 2019, "Wall-attached clusters for the logarithmic velocity law in turbulent pipe flow", *Physics of Fluids*, in press.

Hwang, Y., 2015, "Statistical structure of self-sustaining attached eddies in turbulent channel flow", *Journal of Fluid Mechanics*, Vol. 767, pp. 254–289.

Jiménez, J., and Hoyas, S., 2008, "Turbulent fluctuations above the buffer layer of wall-bounded flows", *Journal of Fluid Mechanics*, Vol. 611, pp. 215–236.

Kim, K., Baek, S. J., and Sung, H. J., 2002, "An implicit velocity decoupling procedure for the incompressible Navier–Stokes equations", *International journal for numerical methods in fluids*, Vol. 38(2), pp. 125-138.

Lee, J. H., 2017, "Large-scale motions in turbulent boundary layers subjected to adverse pressure gradients", *Journal of Fluid Mechanics*, Vol. 810, pp. 323–361.

Lee, J. H., and Sung, H. J., 2009, "Structures in turbulent boundary layers subjected to adverse pressure gradients", *Journal of Fluid Mechanics*, Vol. 639, pp. 101–131.

Lee, M., and Moser, R. D., 2015, "Direct numerical simulation of turbulent channel flow up to $Re_\tau \approx 5200$", *Journal of Fluid Mechanics*, Vol. 774, pp. 395–415.

Lozano-Durán, A., Flores, O., and Jiménez, J., 2012, "The three-dimensional structure of momentum transfer in turbulent channels", *Journal of Fluid Mechanics*, Vol. 694, pp. 100–130.

Maciel, Y., Gungor, A. G., and Simens, M., 2017*a*, "Structural differences between small and large momentum-defect turbulent boundary layers", *International Journal of Heat and Fluid Flow*, Vol. 67, pp. 95–110.

Maciel, Y., Simens, M. P., and Gungor, A. G., 2017*b*, "Coherent Structures in a Non-equilibrium Large-Velocity-Defect Turbulent Boundary Layer", *Flow, Turbulence and Combustion*, Vol. 98(1), pp. 1–20.

Marusic, I., and Monty, J. P., 2019, "Attached Eddy Model of Wall Turbulence", *Annual Review of Fluid Mechanics*, Vol. 51, pp. 49–74.

Marusic, I., and Perry, A. E., 1995, "A wall-wake model for the turbulence structure of boundary layers. Part 2. Further experimental support", *Journal of Fluid Mechanics*, Vol. 298, pp. 389–407.

Örlü, R., Fiorini, T., Segalini, A., Bellani, G., Talamelli, A., and Alfredsson, P. H., 2017, "Reynolds stress scaling in pipe flow turbulence—first results from CICLoPE", *Philosophical Transactions of the Royal Society A: Mathematical, Physical and Engineering Sciences*, Vol. 375(2089), 20160187.

Perry, A. E., and Chong, M. S., 1982, "On the mechanism of wall turbulence", *Journal of Fluid Mechanics*, Vol. 119, pp. 173–217.

Perry, A. E., Henbest, S., and Chong, M. S., 1986, "A theoretical and experimental study of wall turbulence", *Journal of Fluid Mechanics*, Vol. 165, pp. 163–199.

Perry, A. E., and Marusic, I., 1995, "A wall-wake model for the turbulence structure of boundary layers. Part 1. Extension of the attached eddy hypothesis", *Journal of Fluid Mechanics*, Vol. 298, pp. 361–388.

Samie, M., Marusic, I., Hutchins, N., Fu, M. K., Fan, Y., Hultmark, M., and Smits, A. J., 2018, "Fully resolved measurements of turbulent boundary layer flows up to $Re_\tau = 20000$", *Journal of Fluid Mechanics*, Vol. 851, pp. 391–415.

Smits, A. J., McKeon, B. J., & Marusic, I., 2011, "High–Reynolds number wall turbulence", *Annual Review of Fluid Mechanics*, Vol. 43, pp. 353–375

Townsend, A. A., 1976, *The structure of turbulent shear flow*, Cambridge university press.

Vallikivi, M., Hultmark, M., and Smits, A. J., 2015, "Turbulent boundary layer statistics at very high Reynolds number", *Journal of Fluid Mechanics*, Vol. 779, pp. 371–389.

Yoon, M., Hwang, J., and Sung, H. J., 2018, "Contribution of large-scale motions to the skin friction in a moderate adverse pressure gradient turbulent boundary Layer", *Journal of Fluid Mechanics*, Vol. 848, pp. 288–311.